AIP | Physics of Plasmas

Enhanced coupling of the fast wave to electrons through mode conversion to the ion hybrid wave

C. N. Lashmore-Davies, V. Fuchs, A. K. Ram, and A. Bers

Citation: Phys. Plasmas **4**, 2031 (1997); doi: 10.1063/1.872369
View online: http://dx.doi.org/10.1063/1.872369
View Table of Contents: http://pop.aip.org/resource/1/PHPAEN/v4/i6
Published by the American Institute of Physics.

Related Articles

The effects of neutral gas heating on H mode transition and maintenance currents in a 13.56MHz planar coil inductively coupled plasma reactor
Phys. Plasmas 19, 093501 (2012)

Collisionless inter-species energy transfer and turbulent heating in drift wave turbulence
Phys. Plasmas 19, 082309 (2012)

Development of a low-energy and high-current pulsed neutral beam injector with a washer-gun plasma source for high-beta plasma experiments
Rev. Sci. Instrum. 83, 083504 (2012)

A stochastic mechanism of electron heating
Phys. Plasmas 19, 082506 (2012)

Toroidal ripple transport of beam ions in the mega-ampère spherical tokamak
Phys. Plasmas 19, 072514 (2012)

Additional information on Phys. Plasmas

Journal Homepage: http://pop.aip.org/
Journal Information: http://pop.aip.org/about/about_the_journal
Top downloads: http://pop.aip.org/features/most_downloaded
Information for Authors: http://pop.aip.org/authors

ADVERTISEMENT

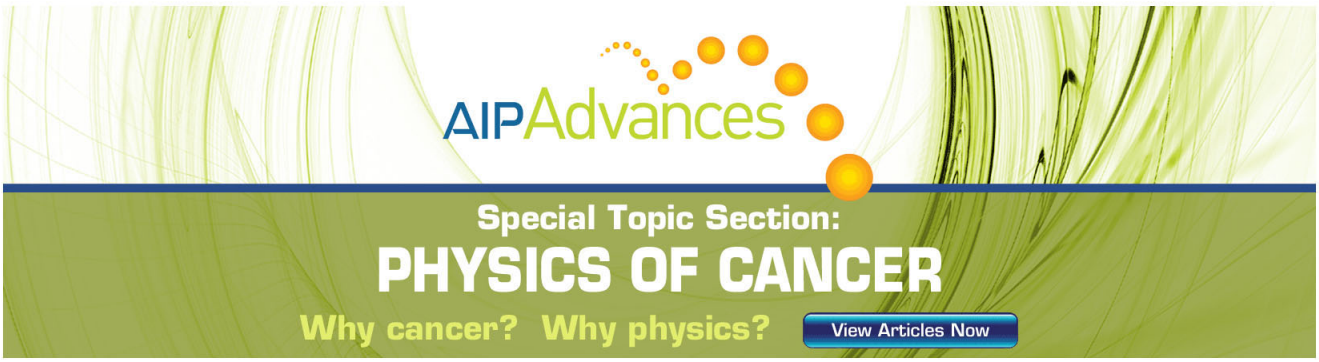

Downloaded 31 Oct 2012 to 194.81.223.66. Redistribution subject to AIP license or copyright; see http://pop.aip.org/about/rights_and_permissions

Enhanced coupling of the fast wave to electrons through mode conversion to the ion hybrid wave

C. N. Lashmore-Davies
United Kingdom Atomic Energy Authority (UKAEA) (UKAEA/Euratom Fusion Association) Fusion, Culham, Abingdon, Oxon, OX14 3DB, United Kingdom

V. Fuchs
Centre Canadien de Fusion Magnétique, 1804 Montée Ste Julie, Varennes, Québec, J3X 1S1, Canada

A. K. Ram and A. Bers
Plasma Fusion Center, Massachusetts Institute of Technology, Cambridge, Massachusetts 02139

(Received 13 August 1996; accepted 14 March 1997)

An analysis of ion cyclotron resonance heating in a plasma containing two ion species is given. Particular emphasis is placed on the important case of comparable concentrations of the two species. The properties of ion-Bernstein waves in such a plasma are discussed. A summary of the cutoff–resonance (Budden) and cutoff–resonance–cutoff (triplet) configurations is given and an analytic expression obtained for the Budden transmission coefficient (relevant also to the triplet case), which is valid for any concentration ratio of the two-ion species. A formula for the damping coefficient of the ion hybrid wave is obtained and a ray tracing code is used to illustrate the absorption of this mode by electrons close to the two-ion hybrid resonance. The reduced, second-order fast wave equation is solved numerically, illustrating the transition from strong electron heating through mode conversion at the two-ion hybrid resonance to direct electron damping of the fast wave in a high beta plasma. [S1070-664X(97)02706-7]

I. INTRODUCTION

Ion cyclotron heating is used in many present generation magnetic fusion experiments and is one of the auxiliary heating methods under consideration for the International Thermonuclear Experimental Reactor[1] (ITER). Fast waves in the ion cyclotron range of frequencies can interact with both electrons and ions. Ion heating occurs in the vicinity of the ion cyclotron resonances, whereas electron heating requires substantial values of the electron beta. For current drive applications, it is of interest to choose conditions such that the incident fast wave damps predominantly on the electrons. Such conditions can be achieved either by operating below all ion cyclotron frequencies or by working at a higher frequency such that only the weakly absorbing high ion cyclotron harmonics (say three and above) are present in the plasma. While ITER will achieve these high electron betas, present experiments do not reach conditions for which the fast wave undergoes strong single pass absorption on the electrons.

In this paper, we analyze another possibility. This scheme is based on the mode conversion that can occur when the two-ion hybrid resonance exists in the plasma. Since the fast wave antenna is situated on the low-field side of present large tokamaks, the occurrence of the two-ion hybrid resonance normally leads to strong reflection of the fast wave from the associated hybrid cutoff. This is particularly true for D(H) plasmas. When the hybrid resonance is well separated from the minority (hydrogen) resonance, strong reflection occurs and very little mode conversion is produced. If $k_{\|}$ is increased, or the minority concentration is reduced, so that the minority and hybrid resonances overlap, reflection is reduced, strong minority ion cyclotron damping occurs, and, again, there is very little mode conversion. For this reason, Ram *et al.*[2] concentrated on small hydrogen concentrations and small values of the parallel wave-number $k_{\|}$ in their discussion of current drive by mode converted ion Bernstein waves.

The fraction of fast wave energy incident from the low-field side, which can be mode converted, depends on the distance between the hybrid cutoff and resonance positions. Jacquinot *et al.*[3] drew attention some time ago to the sensitivity of this distance to $k_{\|}$. Recently, Majeski *et al.*[4] have again emphasized this point by noting that significant mode conversion can occur in D–T, D–^{3}He plasmas of equal ion concentrations and high values of the fast wave parallel wave number, $k_{\|}$. In addition, Majeski *et al.*[4] have also drawn attention to the effect that the fast wave cutoff on the high-field side has on the mode conversion, which occurs in the vicinity of the two-ion hybrid resonance. Two configurations must be considered. The first is the well-known one of a cutoff–resonance first treated by Budden,[5] which is relevant when the cutoff on the high-field side is not present in the plasma. The second refers to the case of three critical points, arising when the high-field side cutoff is present in the plasma (the usual situation, in fact). This cutoff–resonance–cutoff triplet was emphasized by Majeski *et al.* and solved in the two-ion hybrid context by Fuchs *et al.*[6] For the Budden case, the condition for 50% transmission corresponds to the maximum

Downloaded 31 Oct 2012 to 194.81.223.66. Redistribution subject to AIP license or copyright; see http://pop.aip.org/about/rights_and_permissions

fraction of 25% mode converted energy in a single transit. In the case of the triplet, the mode converted fraction can be 100% (Refs. 4, 6, and 7) for a single transit, provided there is no other damping. This condition depends on the species mix and the value of the parallel wave number.

For a plasma with two-ion species present in comparable proportions, it is well known that the two-ion hybrid resonance is well separated from the regions of ion cyclotron resonance.[8,9] Hence, both the fast wave and the mode converted wave are undamped by the ions in the region of the hybrid resonance unless a population of energetic ions is present. This point will be quantified later. In the present paper, we are more concerned with electron absorption and we shall show that the mode converted wave is damped strongly by the electrons in the vicinity of the two-ion hybrid resonance. Thus, for conditions corresponding to efficient mode conversion, strong localized electron heating can be expected. Furthermore, since the localization of the heating is governed by the position of the two-ion hybrid resonance, both on- and off-axis heating can be produced. These features have already been observed by Majeski *et al.*[4] on the Tokamak Fusion Test Reactor[10] (TFTR).

The plan of the paper is as follows: Section II contains a general review of the dispersion relation for the fast wave in a hot plasma. It is shown that for a cold plasma, the fast wave couples to the shear Alfvén wave at the two-ion hybrid resonance, whereas in a hot plasma the fast wave couples to the ion hybrid wave (a member of the family of ion Bernstein waves) when the plasma beta exceeds the electron-to-ion mass ratio. Section III provides a discussion of the properties of ion-Bernstein waves in a plasma containing two ion species. Particular attention is focused on the ion hybrid wave. Section IV is concerned with the behavior of the fast wave at the two-ion hybrid resonance. A general analytic expression is given for the transmission coefficient for a plasma with two-ion species for any concentration ratio. The Budden and triplet configurations are briefly compared. In Sec. V, the fast wave equation containing the two-ion hybrid resonance and all ion and electron damping terms is given. In Sec. VI, an approximate local dispersion relation is derived, which enables the damping of the mode converted ion hybrid wave to be calculated. The damping of the ion hybrid wave is also computed with the aid of a toroidal ray tracing code. A quantitative analysis of the damping of the fast wave obtained from integration of the fast wave equation is given in Sec. VII. A comparison of the power mode converted with the power dissipated outside the hybrid resonance region is also presented. The transition from electron heating via mode conversion to direct electron damping of the fast wave as the electron beta rises is quantified. Parameters appropriate to the Joint European Torus[11] (JET) and TFTR are chosen. The main contributions of the paper are contained in Secs. III, IV, VI, and VII. Finally, a summary and conclusions are given in Sec. VIII.

II. THE REDUCED DISPERSION RELATION

Let us begin our discussion from the full, hot plasma, electromagnetic dispersion relation. The dispersion relation is obtained in the usual way from the linearized set of Maxwell's equations and the Vlasov equation. Formally, we write

$$(n^2\underline{I}-\mathbf{nn}-\underline{\epsilon})\mathbf{E}=0, \tag{1}$$

where $\underline{\epsilon}(\omega,\mathbf{k})$ is the hot plasma dielectric tensor calculated assuming that all species of particles have a Maxwellian distribution function. We assume a harmonic time and space dependence of the form $\exp i(\mathbf{k}\cdot\mathbf{x}-\omega t)$, where $k=(k_\perp,0,k_\parallel)$. In Eq. (1), $\mathbf{n}=c\mathbf{k}/\omega$ and $n^2=n_\perp^2+n_\parallel^2$. The dispersion relation is obtained by setting the determinant of Eq. (1) to zero. The dispersion relation can be written

$$\begin{aligned}(n_\perp^2-\epsilon_{zz})\{&(n_\parallel^2-\epsilon_{xx})(n_\parallel^2-\epsilon_{yy})+\epsilon_{xy}^2+(n_\parallel^2-\epsilon_{xx})n_\perp^2\}\\&-(n_\parallel^2-\epsilon_{yy})n_\parallel^2n_\perp^2-n_\parallel^2n_\perp^4\\&=\epsilon_{yz}\{\epsilon_{xy}(n_\perp n_\parallel+\epsilon_{xz})-\epsilon_{yz}(n_\parallel^2-\epsilon_{xx})\}\\&\quad+\epsilon_{xz}\{\epsilon_{xy}\epsilon_{yz}+(n_\perp n_\parallel+\epsilon_{xz})(n^2-\epsilon_{yy})\}\\&\quad+n_\parallel n_\perp\{\epsilon_{xy}\epsilon_{yz}+\epsilon_{xz}(n^2-\epsilon_{yy})\}.\end{aligned} \tag{2}$$

In the limit of a cold plasma, the right-hand side of Eq. (2) vanishes. Comparing the order of magnitude of the terms on the right-hand side with the dominant terms on the left-hand side, we find that, to a first approximation, the right-hand side can be neglected. For example, the ratio of the term $\epsilon_{yz}^2\epsilon_{xx}$ to $\epsilon_{zz}\epsilon_{xx}\epsilon_{yy}$ is approximately $k_\perp^2v_{Ti}^2/\Omega_i^2$, which is small for thermal ions. We can simplify Eq. (2) further by taking advantage of the dominance of the ϵ_{zz} element in the ion cyclotron range of frequencies. Retaining only those terms proportional to ϵ_{zz}, we obtain the usual fast wave approximation, which neglects the effect of the parallel electric field. In Sec. VI we shall generalize the fast wave approximation to include the parallel electric field through the retention of the off-diagonal terms on the right-hand side of Eq. (2). The final simplification of Eq. (2) is made through the usual finite Larmor radius expansion. We write the elements of the dielectric tensor to first order in $\lambda_j=k_\perp^2v_{Tj}^2/2\Omega_j^2$, where $v_{Tj}^2=2T_j/m_j$, the subscript j refers to the jth charge species, and Ω_j is the cyclotron frequency of the species. The elements can be obtained from Stix[12] and are

$$\epsilon_{xx}=S_0+\frac{1}{2}\,\sigma_1n_\perp^2, \tag{3}$$

$$\epsilon_{yy}=S_0+\frac{1}{2}\,\sigma_2n_\perp^2, \tag{4}$$

$$\epsilon_{xy}=iD_0+\frac{i}{2}\,\delta n_\perp^2. \tag{5}$$

The quantities S_0 and D_0 are given by

Downloaded 31 Oct 2012 to 194.81.223.66. Redistribution subject to AIP license or copyright; see http://pop.aip.org/about/rights_and_permissions

$$S_0 = 1 + \sum_j \frac{\omega_{pj}^2}{2\omega^2}\,\zeta_{0j}[Z(\zeta_{1j}) + Z(\zeta_{-1j})], \tag{6}$$

$$D_0 = -\frac{\omega_{pe}^2}{\omega\Omega_e} + \sum_j \frac{\omega_{pj}^2}{2\omega^2}\,\zeta_{0j}[Z(\zeta_{1j}) - Z(\zeta_{-1j})], \tag{7}$$

where

$$\zeta_{nj} = (\omega - n\Omega_j)/k_\parallel v_{T_j}. \tag{8}$$

In the above expressions, Ω_j and Ω_e are all positive quantities

$$\sigma_1 = \sum_j \frac{\omega_{pj}^2}{\omega^2}\,\zeta_{0j}\,\frac{v_{Tj}^2}{2\Omega_j^2}\,\frac{\omega^2}{c^2}\,[-Z(\zeta_{1j}) - Z(\zeta_{-1j}) + Z(\zeta_{2j}) + Z(\zeta_{-2j})], \tag{9}$$

$$\sigma_2 = \sum_j \frac{\omega_{pj}^2}{\omega^2}\,\zeta_{0j}\,\frac{v_{Tj}^2}{2\Omega_j^2}\,\frac{\omega^2}{c^2}\,[-3Z(\zeta_{1j}) - 3Z(\zeta_{-1j}) + 4Z(\zeta_{0j}) + Z(\zeta_{2j}) + Z(\zeta_{-2j})] + \frac{\omega_{pe}^2}{\omega^2}\,\zeta_{0e}\,\frac{v_{Te}^2}{2\Omega_e^2}\,\frac{\omega^2}{c^2}\,4Z(\zeta_{0e}), \tag{10}$$

$$\delta = \sum_j \frac{\omega_{pj}^2}{\omega^2}\,\zeta_{0j}\,\frac{v_{Tj}^2}{2\Omega_j^2}\,\frac{\omega^2}{c^2}\,[-2Z(\zeta_{1j}) + 2Z(\zeta_{-1j}) + Z(\zeta_{2j}) - Z(\zeta_{-2j})]. \tag{11}$$

Neglecting the right-hand side of Eq. (2) and substituting Eqs. (3)–(5) into Eq. (2), a sixth-order equation is obtained. This can be reduced to a fourth-order equation by the usual approximation of neglecting electron inertia. The dominant terms on the left-hand side of Eq. (1) are those proportional to ϵ_{zz}. The resulting fourth-order equation is

$$\left(\frac{1}{2}\,\sigma_1 + \frac{\delta^2}{4} - \frac{\sigma_1\sigma_2}{4}\right) n_\perp^4 + \left[S_0 - n_\parallel^2 - \frac{1}{2}\,(\sigma_1 + \sigma_2) \times (S_0 - n_\parallel^2) + \delta D_0\right] n_\perp^2 - (S_0 - D_0 - n_\parallel^2) \times (S_0 + D_0 - n_\parallel^2) = 0. \tag{12}$$

This equation is valid provided $\mu_0 n_0 T_i/B_0^2 > m_e/m_i$. The significance of Eq. (12) is the following: For a cold plasma, the fast Alfvén wave couples to the shear Alfvén wave in the vicinity of the two-ion hybrid resonance, given by $S_0 = 0$. However, for a hot plasma, the fast wave couples to the ion hybrid wave, which is a member of the family of ion-Bernstein waves. The dispersion relation given in Eq. (12) will be used as the basis for an approximate analysis of the fast wave in a multi-ion species plasma in the presence of the two-ion hybrid resonance. Before discussing the propagation and absorption of the fast wave, the properties of ion-Bernstein waves in a two-ion species plasma will be considered.

III. ION BERNSTEIN WAVES IN A TWO-ION SPECIES PLASMA

In a hot plasma where $\beta_i > m_e/m_i$, the fast wave couples to the ion hybrid wave near to the two-ion hybrid resonance. Since most previous discussions of ion-Bernstein waves have been restricted to a single ion species, it is worthwhile to consider the important case of a two-ion species plasma. Ono[13] has previously given a discussion of the cold, electrostatic wave propagating obliquely to the magnetic field near the two-ion hybrid frequency. Here, we provide a complementary discussion to that of Ono[13] in that we restrict the analysis of this section to perpendicular propagation but include the hot plasma effects. We also include electromagnetic effects, which introduce the coupling of the electrostatic wave to the compressional or fast Alfvén wave.

The electrostatic dispersion relation for ion-Bernstein waves propagating at right angles to a uniform magnetic field can be written in the form[12]

$$1 - 2\sum_j \frac{\omega_{pj}^2}{\omega^2} \sum_{n=1}^{\infty} \frac{n^2 e^{-\lambda_j}}{\lambda_j}\, I_n(\lambda_j)\, \frac{\omega^2}{(\omega^2 - n^2\Omega_j^2)} = 0, \tag{13}$$

where the summation over j is over all ion species and the electrons. The effect of the electrons can be neglected for long wavelengths ($\lambda_j \ll 1$) but must be included for short wavelengths ($\lambda_j \gg 1$). Consider the case of a two-ion species plasma. The dispersion relation can be written in the form

$$1 + \frac{\omega_{pe}^2}{\Omega_e^2} - 2\sum_{n=1}^{\infty}\left[\Lambda_{1n}\,\frac{n^2\omega_{p1}^2}{(\omega^2 - n^2\Omega_1^2)} + \Lambda_{2n}\,\frac{n^2\omega_{p2}^2}{(\omega^2 - n^2\Omega_2^2)}\right] = 0, \tag{14}$$

where only the $n = 1$ electron term has been included, to zero order in λ_e, since $\lambda_e \ll 1$. The subscripts 1 and 2 denote the two-ion species and

$$\Lambda_{jn} = \frac{e^{-\lambda_j}}{\lambda_j}\, I_n(\lambda_j); \quad j = 1,2. \tag{15}$$

Combining the two ion terms, the dispersion relation becomes

$$1 + \frac{\omega_{pe}^2}{\Omega_e^2} - 2\sum_{n=1}^{\infty} n^2(\Lambda_{1n}\omega_{p1}^2 + \Lambda_{2n}\omega_{p2}^2) \times \frac{(\omega^2 - n^2\Omega_{hn}^2)}{(\omega^2 - n^2\Omega_1^2)(\omega^2 - n^2\Omega_2^2)} = 0, \tag{16}$$

where

$$\Omega_{hn}^2 = \frac{(\Lambda_{1n}\omega_{p1}^2\Omega_2^2 + \Lambda_{2n}\omega_{p2}^2\Omega_1^2)}{(\Lambda_{1n}\omega_{p1}^2 + \Lambda_{2n}\omega_{p2}^2)}. \tag{17}$$

For $\lambda_1 \ll 1$, $\lambda_2 \ll 1$ we have $\Lambda_{11} \simeq \frac{1}{2}$, $\Lambda_{21} \simeq \frac{1}{2}$, giving

$$\Omega_{h1}^2 \simeq \frac{(\omega_{p1}^2\Omega_2^2 + \omega_{p2}^2\Omega_1^2)}{(\omega_{p1}^2 + \omega_{p2}^2)}, \tag{18}$$

which will be recognized as the two-ion hybrid resonance frequency for a cold plasma.

For a single ion species plasma, the lowest frequency ion-Bernstein wave in the long wavelength limit ($\lambda_j \to 0$)

Downloaded 31 Oct 2012 to 194.81.223.66. Redistribution subject to AIP license or copyright; see http://pop.aip.org/about/rights_and_permissions

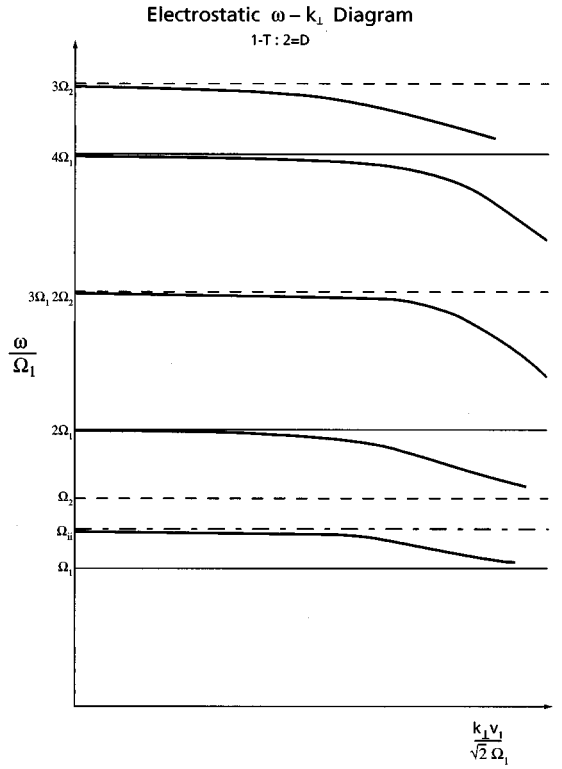

FIG. 1. The electrostatic dispersion relation for ion-Bernstein waves propagating at right angles to a uniform magnetic field in a plasma with equal concentrations of deuterium and tritium. The deuterium concentration, $n_D = 2.5\times10^{19}$ m^{-3}, the magnetic field, $B_0 = 3$ T, and the ion temperatures are both taken as 10 keV.

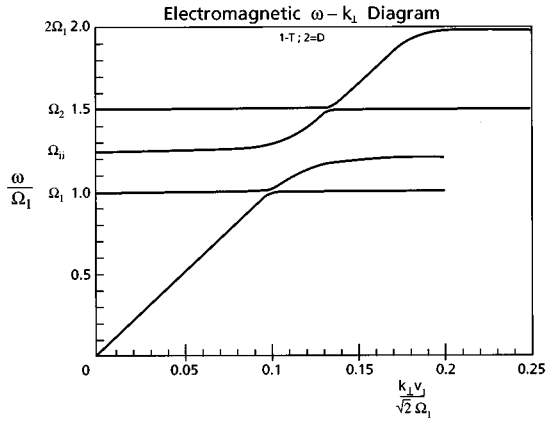

FIG. 2. The electromagnetic dispersion relation for propagation at right angles to the magnetic field. The parameters are the same as Fig. 1.

occurs just below the second-harmonic cyclotron frequency, $\omega \lesssim 2\Omega$. However, for two-ion species it can be seen, on examination of Eq. (16), that the lowest frequency solution in the long wavelength limit begins just below the two-ion hybrid frequency. No solution is possible in the long wavelength limit for $\Omega_{h1} < \omega < \Omega_2$. In the short wavelength limit, $\lambda_j \gg 1, \omega \to \Omega_1$ from above, where we assume that $\Omega_2 > \Omega_1$. We distinguish this wave from other Bernstein waves by referring to it as the ion hybrid wave. The frequency, Ω_{h1}, introduces this additional mode because $\Lambda_{j1}(\lambda_j) \to \frac{1}{2}$ as $\lambda_j \to 0$, whereas all other $\Lambda_{jn}(\lambda_j) \to 0$ as $\lambda_j \to 0$. Thus, the ion hybrid wave lies in the frequency range $\Omega_1 < \omega < \Omega_{h1}$. No solutions occur between Ω_{h1} and Ω_2.

The first ion-Bernstein wave, for long wavelengths, begins just below $2\Omega_1$ (provided $2\Omega_1 \neq \Omega_2$) and tends asymptotically to Ω_2 from above for short wavelengths. The particular case of a deuterium–tritium plasma with equal concentrations of deuterium and tritium is shown in Fig. 1. The first few ω versus $k_\perp$ curves are shown. The lowest branch is the ion hybrid wave. The first ion-Bernstein wave starts from its cutoff just below $2\Omega_1$ and tends asymptotically to Ω_2 from above. The next ion-Bernstein wave begins just below $2\Omega_2$ (which is, of course, degenerate with $3\Omega_1$) and tends asymptotically to $2\Omega_1$. The following ion-Bernstein wave has its cutoff just below $4\Omega_1$ and ends on $2\Omega_2$ (which is also $3\Omega_1$). The last ion-Bernstein wave shown starts just below $3\Omega_2$ and tends asymptotically to $4\Omega_1$. The dispersion curves shown in Fig. 1 illustrate the crucial difference between the ion hybrid wave and the ion-Bernstein waves. The ion hybrid wave is the only one which does *not* start from a harmonic of one of the ion cyclotron frequencies. Thus, when a finite value of the parallel wave number is included, all the ion-Bernstein waves will be subject to ion cyclotron damping for values of $k_\perp$ near to the cutoff, which increases in strength as $k_\parallel$ increases. In contrast, the ion hybrid wave (for comparable ion densities) propagates at frequencies between the two-ion cyclotron frequencies and is, therefore, much less susceptible to ion cyclotron damping. The dispersion relation for the ion hybrid wave for oblique propagation is, therefore, well approximated by the dispersion relation for perpendicular propagation. The significance of this property of the ion hybrid wave is that it is, therefore, much more likely to be excited by mode conversion of the fast Alfvén wave in ion cyclotron heating experiments, even for large values of $k_\parallel$, provided the two ion species are present in comparable proportions.

The electromagnetic dispersion relation for propagation at right angles to the magnetic field is shown in Fig. 2, for which the parameters are the same as in Fig. 1. The dispersion curves in Fig. 2 show the strong coupling between the compressional Alfvén wave and the ion hybrid wave and the much weaker coupling at the two ion cyclotron frequencies. This is indicated by the size of the gap between the coupled branches. The cyclotron harmonic waves at the two fundamental cyclotron frequencies are not Bernstein waves but arise from the electromagnetic terms in the dispersion relation. These electromagnetic cyclotron harmonic waves were first analyzed by Akhiezer *et al.*[14] and have also been discussed more recently by Chow *et al.*[15]

IV. MODE CONVERSION OF THE FAST WAVE TO THE ION HYBRID WAVE

An explicit calculation of the mode conversion of the fast Alfvén wave into the ion hybrid wave requires the solution of a fourth-order differential equation. Such a fourth-order equation can be obtained from the (fourth-order) dispersion relation given by Eq. (12). In this section, we will establish the transmission, reflection, and mode conversion coefficients for the fast wave crossing the two-ion hybrid

Downloaded 31 Oct 2012 to 194.81.223.66. Redistribution subject to AIP license or copyright; see http://pop.aip.org/about/rights_and_permissions

resonance in a plasma with two ion species in arbitrary proportions and for oblique propagation. Since we shall be most interested in the case where the two-ion species are present in comparable proportions, ion cyclotron damping will be negligible in the region of the two-ion hybrid resonance. In view of this, we can obtain this information from the cold plasma model by solving the Budden equation.

Thus, neglecting the finite Larmor radius corrections in Eq. (12), we obtain the well-known fast wave refractive index

$$n_\perp^2=\frac{(S_0-D_0-n_\parallel^2)(S_0+D_0-n_\parallel^2)}{(S_0-n_\parallel^2)}. \tag{19}$$

The cold plasma approximation is now obtained by expanding S_0 and D_0 asymptotically to obtain

$$n_\perp^2=\frac{\left[\dfrac{\omega_{p1}^2}{\Omega_1(\omega+\Omega_1)}+\dfrac{\omega_{p2}^2}{\Omega_2(\omega+\Omega_2)}-n_\parallel^2\right]\left[\dfrac{\omega_{p1}^2}{\Omega_1(\omega-\Omega_1)}+\dfrac{\omega_{p2}^2}{\Omega_2(\omega-\Omega_2)}+n_\parallel^2\right]}{\left[\dfrac{\omega_{p1}^2}{(\omega^2-\Omega_1^2)}+\dfrac{\omega_{p2}^2}{(\omega^2-\Omega_2^2)}+n_\parallel^2\right]}. \tag{20}$$

We expand the dispersion relation about the position of the ion hybrid resonance, where the wave frequency, ω, satisfies the resonance condition

$$\omega^2=\frac{\omega_{p1}^2\Omega_2^2+\omega_{p2}^2\Omega_1^2}{\omega_{p1}^2+\omega_{p2}^2}\equiv\Omega_{ii}^2. \tag{21}$$

The equilibrium magnetic field is assumed to vary as $B_0(x)=B_0(R)(1-(x/R))$. After some algebra, Eq. (20) can be written as

$$\frac{c_A^2k_\perp^2}{\Omega_{ii}^2}\simeq\frac{k_0^2(\xi-\xi_c)}{(\xi-\xi_R)}, \tag{22}$$

where

$$k_0^2=\left(\frac{\Omega_{ii}}{\Omega_1}+1\right)\left(\frac{\Omega_{ii}}{\Omega_2}+1\right)\left[\frac{\rho_1}{\left(\dfrac{\Omega_{ii}}{\Omega_1}+1\right)(\rho_1+\rho_2)}+\frac{\rho_2}{\left(\dfrac{\Omega_{ii}}{\Omega_2}+1\right)(\rho_1+\rho_2)}-N_\parallel^2\right], \tag{23}$$

$$\xi_c=-R_A-\frac{R_A(\omega_{p1}^2\Omega_2+\omega_{p2}^2\Omega_1)}{(\omega_{p1}^2+\omega_{p2}^2)^{1/2}(\omega_{p1}^2\Omega_2^2+\omega_{p2}^2\Omega_1^2)^{1/2}}-R_AN_\parallel^2\left(\frac{\Omega_{ii}}{\Omega_1}-1\right)\left(\frac{\Omega_{ii}}{\Omega_2}-1\right), \tag{24}$$

$$\xi_R=-R_AN_\parallel^2\left(\frac{\Omega_{ii}^2}{\Omega_1^2}-1\right)\left(\frac{\Omega_{ii}^2}{\Omega_2^2}-1\right), \tag{25}$$

and $\xi=\Omega_{ii}x/c_\mathrm{A}$, $R_A=R\Omega_{ii}/c_\mathrm{A}$, and $N_\parallel=c_Ak_\parallel/\Omega_{ii}$. The Alfvén speed c_A for a two-ion species plasma with arbitrary densities is given by $c_\mathrm{A}^2=B_0^2/[\mu_0(\rho_1+\rho_2)]$, where $\rho_{1,2}$ are the mass densities of the two ion species. Taking the inverse Fourier transform of Eq. (22), we obtain Budden's equation for a general, two-ion species plasma, in the ion hybrid resonance region

$$\frac{d^2E_y}{d\xi^2}+\frac{k_0^2(\xi-\xi_c)E_y}{(\xi-\xi_R)}=0. \tag{26}$$

It can be seen that Eq. (26) is symmetric in the subscripts 1 and 2, as it should be since the two ion species have been treated on an equal footing. The equation applies to any two-ion species, for any concentration ratio. However, it is most relevant to the case where the ion concentrations are comparable because of the neglect of ion cyclotron damping. The transmission coefficient for the fast wave crossing the two-ion hybrid resonance is immediately obtained from Eq. (26) and is given by[5]

$$T=\exp[-\pi|\xi_C-\xi_R|k_0]. \tag{27}$$

It is well known that the proportion of energy reflected from the cutoff associated with the resonance for a wave incident from the low magnetic-field side is given by $R=(1-T)^2$ and, therefore, that the fraction of mode converted energy is $M=T(1-T)$. Hence, according to the Budden model, the maximum fraction of the energy incident from the low-field side that can be mode converted in a single transit of the resonance is 25%. This occurs when 50% of the incident energy is transmitted across the resonance. The optimum conditions for a given species mix can be obtained from Eq. (27).

The dependence of the optimum conditions on the ion species, concentrations, and parallel wave number was noted by Jacquinot *et al.*[3] However, Majeski *et al.*[4] have recently drawn attention to the fact that the full wave treatment of the two-ion hybrid resonance and cutoff region should also be extended to include the effect of the fast wave cutoff on the high-field side. This configuration of three critical points, as opposed to the two treated in the Budden equation, is referred to as a triplet. As $k_\parallel$ is varied, the fast wave cutoff

Downloaded 31 Oct 2012 to 194.81.223.66. Redistribution subject to AIP license or copyright; see http://pop.aip.org/about/rights_and_permissions

moves relative to the hybrid resonance and its associated cutoff, which also move relative to each other (but at a much slower rate).

The triplet configuration for a two-ion species plasma was solved by Fuchs *et al.*[6] An interesting feature of the solutions (both analytic and numerical) is that the Budden transmission coefficient again appears in the analysis. In fact, the condition for maximum mode conversion in the triplet configuration again corresponds to a value of 0.5 for the Budden transmission coefficient and, in addition, to a phase condition. Because of the second cutoff on the high-field side, there is no transmitted energy for the triplet case. The incident energy is either reflected or mode converted. Depending on the separation of the high-field-side cutoff and the resonance, either the mode conversion is enhanced and the reflection reduced, or vice versa. This separation is a function of the parallel wave number. Hence, the mode conversion and reflection coefficients exhibit oscillatory behavior as a function of the parallel wave number. For a case with no other losses, the optimum condition gives rise to 100% mode conversion for a single interaction of the incident wave with the resonance. A similar result was previously obtained by Ngan and Swanson,[16] who included the effect of wall reflection of the transmitted energy back to the resonance region. These authors also showed that 100% mode conversion could occur for low-field-side incidence.

The triplet configuration should be used whenever the high-field-side fast wave cutoff is present in the plasma, which is usually the case. If the cutoff is not present in the plasma, then the Budden configuration should be used. Even in this case, the transmitted energy can be returned to the resonance region by reflection from the wall. For this situation, the single pass result can be enhanced by multiple passes of the resonance region, but a quantitative assessment requires an explicit calculation of the wall reflection from both the low- and high-field side of the resonance.[17] For this more involved calculation, another key ingredient would be the strength of the damping outside the two-ion hybrid resonance region.

V. THE DAMPING OF THE FAST WAVE

The main emphasis in the present paper is on the case of two-ion species with comparable densities. The cold plasma model discussed in the previous section provides an accurate description of the fast wave in the hybrid resonance region. The validity condition for the cold model is that the ion cyclotron resonances do not overlap the hybrid resonance zone. As an illustrative example, we consider a deuterium–tritium plasma with equal concentrations. For this case, the two-ion hybrid resonance frequency is $\Omega_{ii}=(\Omega^{\mathrm{D}}\Omega_{\mathrm{T}})^{1/2}$. The condition for a deuteron to be in fundamental cyclotron resonance at the two-ion hybrid resonance is, therefore, given by $(\Omega_{\mathrm{D}}\Omega_{\mathrm{T}})^{1/2}-\Omega_{\mathrm{D}}-k_{\|}v_{\mathrm{TD}}=0$. For a given value of $k_{\|}$, this condition can be written as $v_{\mathrm{TD}}=[1-(\Omega_{\mathrm{T}}/\Omega_{\mathrm{D}})^{1/2}]\times(\Omega_{\mathrm{D}}/k_{\|})$. Expressing this in terms of the deuteron temperature, T_{D}, we obtain $T_{\mathrm{D}}(\mathrm{MeV})=9.35/k_{\|}^2$. Hence, for $k_{\|}\leqslant 3\ \mathrm{m}^{-1}$ only MeV deuterons are energetic enough to produce overlap of the cyclotron and hybrid resonances. For larger values of $k_{\|}$, in the range $3-10\ \mathrm{m}^{-1}$, deuterons must still have a temperature of the order or in excess of 100 keV to produce overlap with the hybrid resonance.

Even if cyclotron damping can be ignored in the hybrid resonance region, a fast wave launched form the low-field side will inevitably cross regions of ion cyclotron resonance. In order to be able to calculate the proportion of launched fast wave power, which can be transferred to the electrons through mode conversion at the two-ion hybrid resonance, the fast wave equation must be generalized to include all damping mechanisms, both ion and electron. This generalization has been carried out by Fuchs *et al.*[6] and is given by

$$\frac{d^2E_y}{dx^2}+\frac{\omega^2}{c^2}\left[\epsilon_{yy}-n_{\|}^2+\frac{\epsilon_{yz}^2}{\epsilon_{zz}}+\frac{[\epsilon_{xy}+\epsilon_{yz}(n_{\|}n_{\perp c}+\epsilon_{xz})/\epsilon_{zz}]^2}{[\epsilon_{xx}-n_{\|}^2-(n_{\|}n_{\perp c}+\epsilon_{xz})^2/\epsilon_{zz}]}\right]E_y=0, \tag{28}$$

where $n_{\perp c}$ is the cold, nonresonant fast wave refractive index. The above Eq. (28) is obtained from Eqs. (4), (9a)–(9c), and (10) of Ref. 6. The electron dissipation of the fast wave is dominated by the terms $\epsilon_{yy}^e+(\epsilon_{yz}^e)^2/\epsilon_{zz}^e$ in Eq. (28). Using Eq. (28) to obtain the local dispersion relation, the local dissipation rate of the fast wave due to the electrons is given by

$$\mathrm{Im}(k_{\perp})_{\mathrm{FW}}\simeq\frac{1}{2k_{\perp c}}\frac{\omega_{pe}^2}{c^2}\frac{k_{\perp}^2v_{Te}^2}{2\Omega_e^2}\,\pi^{1/2}\zeta_{oe}e^{-\zeta_{oe}^2}, \tag{29}$$

where the kinetic expressions for ϵ_{yy}^e, ϵ_{yz}^e, and ϵ_{zz}^e have been used (see, for example Ref. 6). The damping rate given in Eq. (29) is in agreement with the approximate value obtained by Porkolab.[18] The fast wave equation given in Eq. (28) satisfies the conservation relation given by Eq. (13) of Ref. 6. This enables the total power absorbed to be written as

$$P_{abs}=-\int_{x_1}^{x_2}\mathrm{Im}(Q)|E_y|^2dx, \tag{30}$$

where x_1 and x_2 are on low- and high-field sides of the interaction region. The potential $Q(x)$ can be obtained from the function multiplying E_y in Eq. (28) and is given explicitly by Eq. (10) in Ref. 6. Results obtained from the integration of Eq. (28) are presented in Sec. VII.

VI. THE DAMPING OF THE ION HYBRID WAVE

In Sec. IV, we considered the optimum conditions to maximize the energy mode converted from the fast wave to the ion hybrid wave. In Sec. V, the competing ion and electron damping mechanisms were included in the fast wave equation to estimate how much power might be lost before the remaining energy reaches the mode conversion region. In this section, we consider the fate of the mode converted ion hybrid wave as it propagates away from the two-ion hybrid resonance region. First, we shall obtain a local dispersion relation, which we shall solve for the local damping rate of

Downloaded 31 Oct 2012 to 194.81.223.66. Redistribution subject to AIP license or copyright; see http://pop.aip.org/about/rights_and_permissions

the ion hybrid wave. We shall then present results obtained from a toroidal, ray tracing code,[19] which allows the mode converted ion hybrid wave to be followed as it propagates away from the coupling region, and its damping to be calculated. The general dispersion relation for the ion hybrid wave in a hot, two-ion species plasma with arbitrary ion concentrations is rather complicated, since the wave exists in both long wavelength, $k_\perp^2\rho_j^2 \ll 1$, and short wavelength, $k_\perp^2\rho_j^2 > 1$, regimes, where ρ_j is the Larmor radius of the jth ion species. In the Appendix, we give the dispersion relation for arbitrary concentrations of two general ion species in the long wavelength regime. First, we shall consider the specific case of a deuterium–tritium plasma in which the ion concentrations and temperatures are assumed to be equal. Since we wish to calculate the electron dissipation of the ion hybrid wave, we start from the full, three-by-three dielectric tensor, but expand the relevant ion terms to first order in λ_j. Again, making use of the dominance of the ϵ_{zz} element in the ion cyclotron range of frequencies, we approximate the full, three-by-three electromagnetic dispersion relation by

$$n_\perp^2(\epsilon_{xx}-n_\parallel^2)-(\epsilon_{yy}^i-n_\parallel^2)(\epsilon_{xx}-n_\parallel^2)-\epsilon_{xy}^2 \simeq \left(\frac{\epsilon_{yz}^2}{\epsilon_{zz}}+\epsilon_{yy}^e\right)(\epsilon_{xx}-n_\parallel^2)+\frac{n_\parallel^2 n_\perp^4}{\epsilon_{zz}}. \tag{31}$$

In the above equation, we have only included the dominant electron damping terms. Note that the ϵ_{yy} element has been separated explicitly into its ion and electron components. The first term on the right-hand side of Eq. (31) describes the electron dissipation of the fast wave and the second term, the electron damping of the ion hybrid wave.[20]

Since the ion hybrid wave is predominantly electrostatic away from the region of coupling to the fast wave, its dissipation is dominated by electron Landau damping. After a significant amount of algebra, the dispersion relation, to first order in the Larmor radius, can be written (see the Appendix)

$$(\omega^2-c_A^2k_\perp^2)\left(\omega^2-\Omega_{ii}^2-\frac{\Omega_T^2}{4}N_\parallel^2+\frac{27}{200}\Omega_T^2\frac{k_\perp^2v_{TD}^2}{\Omega_D^2}\right) -\frac{9}{50}\Omega_T^4\left(\frac{1}{2}-\frac{25}{12}N_\parallel^2-2\frac{k_\perp^2v_{TD}^2}{\Omega_D^2}\right) \simeq\left(\frac{\Omega_D^2}{\omega_{pD}^2}\right)^2\frac{(\omega^2-\Omega_D^2)(\omega^2-\Omega_T^2)\omega^2n_\parallel^2n_\perp^4}{(1+\omega_{pT}^2/\omega_{pD}^2)(1+\rho_T/\rho_D)\Omega_D^2\epsilon_{zz}}, \tag{32}$$

where only the term that dominates the damping of the ion hybrid wave has been retained on the right-hand side of Eq. (32). The numerical coefficients in this equation arise because of the specific choice of a deuterium–tritium plasma with equal concentrations and temperatures. The subscripts D and T, of course, refer to deuterium and tritium quantities. For equal deuterium and tritium concentrations, $\Omega_{ii}^2=\Omega_D\Omega_T$. The remaining quantities in Eq. (32) have already been defined.

We shall now use Eq. (32) to obtain the damping rate of the ion hybrid wave outside the region of coupling to the fast wave. In particular, we shall be concerned with the region where $c_A^2k_\perp^2/\omega^2>1$. Let us first solve Eq. (32) perturbatively for the imaginary part of the frequency by assuming

$$\omega \simeq \Omega_{IH}+\delta\omega, \tag{33}$$

where Ω_{IH} is the solution of the equation

$$\omega^2-\Omega_{ii}^2-\frac{\Omega_T^2}{4}N_\parallel^2+\frac{27}{200}\Omega_T^2\frac{k_\perp^2v_{TD}^2}{\Omega_D^2} -\frac{9}{50}\Omega_T^2\frac{(\frac{1}{2}-\frac{25}{12}N_\parallel^2-(k_\perp^2v_{TD}^2/\Omega_D^2))}{(\Omega_{ii}^2-c_A^2k_\perp^2)}=0. \tag{34}$$

Substituting Eq. (33) into Eq. (32) and extracting the imaginary part, we obtain

$$\mathrm{Im}\ \delta\omega \simeq \frac{6}{50}\left(\frac{\Omega_D^2}{\omega_{pD}^2}\right)^2\frac{(\Omega_{IH}^2-\Omega_D^2)(\Omega_{IH}^2-\Omega_T^2)}{\Omega_{IH}\Omega_{ii}^2} \times\frac{\Omega_{IH}^2}{\Omega_D^2}\frac{n_\parallel^2n_\perp^4}{(N_\perp^2-1)}\frac{k_\parallel^2v_{Te}^2}{2\omega_{pe}^2}\frac{\pi^{1/2}\zeta_{0e}e^{-\zeta_{0e}^2}}{|1+\zeta_{0e}Z(\zeta_{0e})|^2}. \tag{35}$$

To a good approximation, Ω_{IH}^2 can be replaced by Ω_{ii}^2 in Eq. (35). Clearly, Im $\delta\omega<0$ since $(\Omega_{IH}^2-\Omega_D^2)(\Omega_{IH}^2-\Omega_I^2)<0$.

Next, we obtain the spatial damping rate. Since this will be compared with the numerical solution for a D–^{3}He plasma in which $n_{^3He}/n_D=\frac{1}{2}$ and $T_{^3He}=T_D$, we require the corresponding equation to Eq. (32) for this case. This can be written in a similar form (see the Appendix)

$$\left(k_\perp^2-\frac{\omega^2}{c_A^2}\right)\left[k_\perp^2-\frac{224}{9}\frac{\Omega_D^2}{v_{TD}^2}\frac{(\Omega_{ii}^2+\Omega_{^3He}^2N_\parallel^2/16-\omega^2)}{\Omega_{^3He}^2}\right] +\frac{2\Omega_{^3He}^2}{c_A^2}\frac{\Omega_D^2}{v_{TD}^2}\left(\frac{1}{7}-\frac{7}{12}N_\parallel^2-0.367\frac{k_\perp^2v_{TD}^2}{\Omega_D^2}\right) =-\frac{24}{7}\left(\frac{\Omega_D^2}{\omega_{pD}^2}\right)^2\frac{(\omega^2-\Omega_D^2)}{v_{TD}^2}\frac{(\omega^2-\Omega_{^3He}^2)}{c_A^2}\frac{\omega^2}{\Omega_D^2}\frac{n_\parallel^2n_\perp^4}{\epsilon_{zz}}, \tag{36}$$

where $c_A^2=B_0^2/(\mu_0\Sigma_jn_jm_j)$ and $\Omega_{ii}^2=\frac{3}{4}\Omega_{^3He}^2$, for this case. We can again solve Eq. (36) perturbatively by assuming

$$k_\perp=k_+ +\delta k_\perp, \tag{37}$$

where $k_\pm^2$ are the solutions of Eq. (36) with the right-hand side set to zero. k_+^2 corresponds to the ion hybrid wave and k_-^2 to the fast wave. For $c_Ak_\perp^2/\omega^2>1$, $k_+^2 \gg k_-^2$. Substituting Eq. (37) into Eq. (36), we obtain

$$\mathrm{Im}\ \delta k_\perp \simeq \frac{24}{7}\left(\frac{\Omega_D^2}{\omega_{pD}^2}\right)^2\frac{(\omega^2-\Omega_D^2)(\omega^2-\Omega_{^3He}^2)\omega^2n_\parallel^2n_+^2}{2v_{TD}^2c_A^2\Omega_D^2k_+(k_+^2-k_-^2)} \times\frac{k_\parallel^2v_{Te}^2\pi^{1/2}\zeta_{0e}e^{-\zeta_{0e}^2}}{2\omega_{pe}^2|1+\zeta_{0e}Z(\zeta_{0e})|^2}, \tag{38}$$

Downloaded 31 Oct 2012 to 194.81.223.66. Redistribution subject to AIP license or copyright; see http://pop.aip.org/about/rights_and_permissions

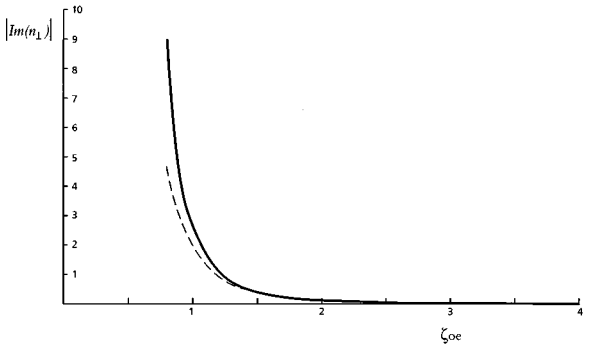

FIG. 3. $|\mathrm{Im}\, n_\perp|$ plotted as a function of $\zeta_{oe} \equiv \omega / k_\parallel v_{Te}$. The solid line is the exact numerical solution of the full electromagnetic dispersion relation and the broken line is the analytic approximation [Eq. (48)].

where n_+ is $ck_\perp / \omega$ evaluated for $k_\perp = k_+$.

Notice that Im $\delta k_\perp < 0$, since the ion hybrid mode is a backward wave. It can also be seen that the damping of the ion hybrid wave becomes stronger as it propagates towards shorter perpendicular wavelengths. Clearly, the ion hybrid wave will only be damped significantly by the electrons for $|\zeta_{0e}| \lesssim 2$.

The approximate spatial damping rate given by Eq. (38) is compared with the exact value obtained from the numerical solution of the full electromagnetic dispersion relation. This comparison is shown in Fig. 3 where Im $n_\perp$ is plotted as a function of $\omega / k_\parallel v_{Te}$. The analytic approximation is in good agreement with the exact numerical result until $k_\perp \rho_i$ for the deuterons and tritons is no longer small, as shown in Fig. 4.

A more detailed picture of the propagation and damping of the ion hybrid wave can be obtained from a toroidal ray tracing code. The results of such a calculation for parameters appropriate to a JET discharge are shown in Figs. 5–8. The electron density is $n_e = 4 \times 10^{19}$ m^{-3}, the magnetic field, $B_0 = 3.45$ T and $T_e = 8$ keV. The two ion species, are deuterium and a 25% concentration of helium-3 (relative to the electron density). The ion temperatures are $T_\mathrm{D} = T_{3_\mathrm{He}} = 5$ keV. The trajectory of the mode converted ion hybrid wave in the poloidal plane is shown in Fig. 5. The wave can be seen to

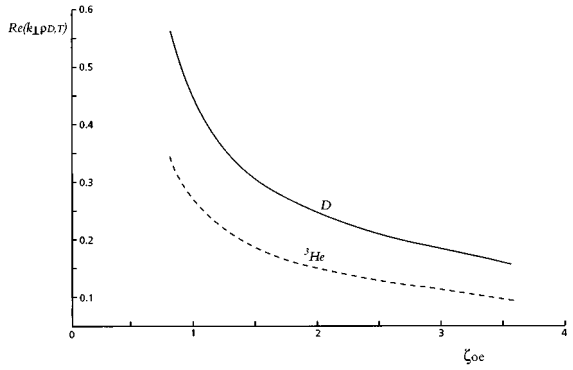

FIG. 4. The real part of the perpendicular wave number of the ion hybrid wave normalized to the Larmor radii of the deuterium and helium-3 ions plotted as a function of $\zeta_{oe} \equiv \omega / k_\parallel v_{Te}$.

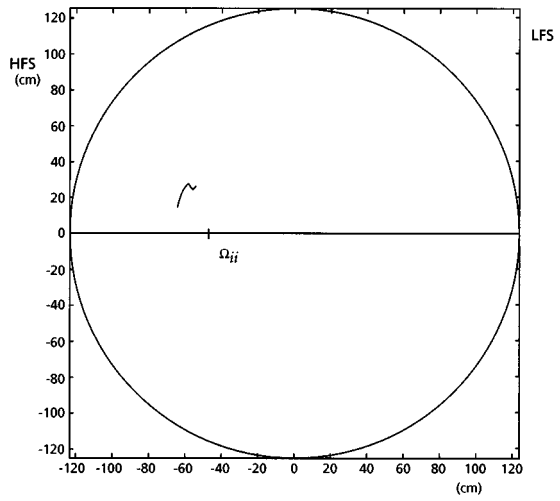

FIG. 5. Poloidal projection of the mode converted ion hybrid wave. The parameters are appropriate to JET: $n_e = 4 \times 10^{19}$ m^{-3}, $B_0 = 3.45$ T, deuterium–helium-3 plasma with 25% helium-3 (relative to the electron density), $T_e = 8$ keV, $T_\mathrm{D} = T_{3_\mathrm{He}} = 5$ keV.

travel only a short distance poloidally before being damped by the electrons. The change of the parallel wave number as the ray propagates is shown in Fig. 6. In Fig. 7, the change of the modulus of the electric field of the ion hybrid wave as it propagates is given. The damping of the wave occurs fairly abruptly and results in complete absorption. The reason for the swift onset of damping is shown in Fig. 8, where the change in the resonant argument $|\zeta_{0e}| = |\omega / k_\parallel v_{Te}|$ is shown. Due to the downshift, this quantity at first increases before decreasing. Strong damping occurs as $|\zeta_{0e}|$ falls below 2.

VII. MODE CONVERSION AND DIRECT DAMPING

In this section, we present the results of integrating Eq. (28) across the plasma. This enables us to assess the compe-

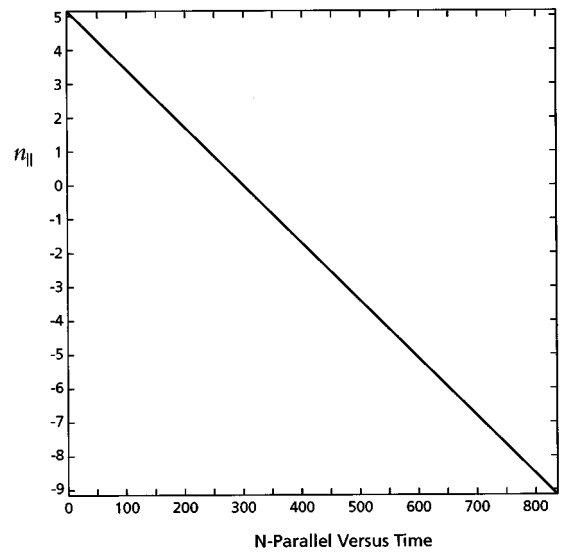

FIG. 6. Change of the parallel refractive index along the ion hybrid ray. The parameters are the same as Fig. 5.

Downloaded 31 Oct 2012 to 194.81.223.66. Redistribution subject to AIP license or copyright; see http://pop.aip.org/about/rights_and_permissions

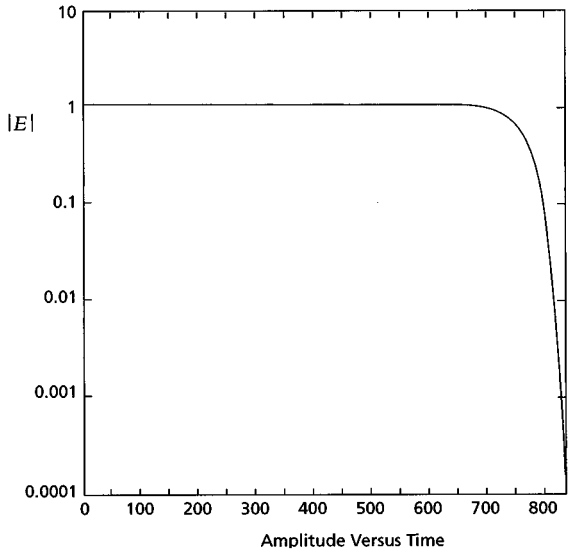

FIG. 7. The change in the modulus of the electric field of the ion hybrid wave along the ray trajectory. The parameters are the same as Fig. 5.

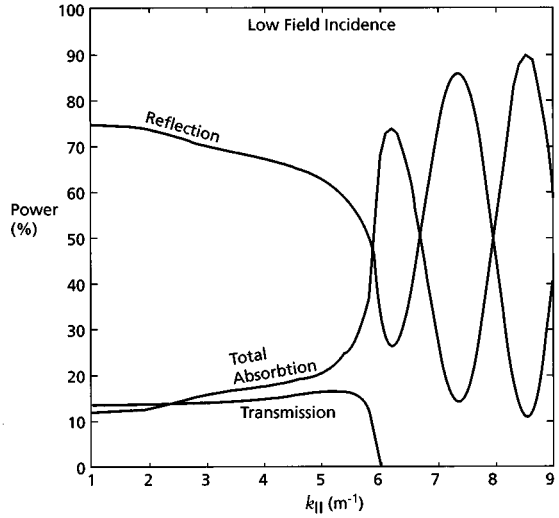

FIG. 9. Transmission, reflection, and total absorption fractions plotted as a function of the parallel wave number for JET conditions: $n_e=4\times10^{19}$ m^{-3}, $B_0=3.45$ T, $R=2.9$ m for a D(^{3}He) plasma with a helium-3 concentration of 25%, $T_e=8$ keV and $T_D=T_{3_{He}}=5$ keV.

tition between direct dissipation of the fast wave and mode conversion at the two-ion hybrid resonance for varying plasma conditions and different tokamaks. We shall give results for three different scenarios, the first appropriate to JET plasmas, the second is relevant to present TFTR plasmas and the third to denser, hotter, plasmas, also in TFTR.

The first set of results are given in Figs. 9–12 and refer to the JET parameters used for the ray tracing results discussed in the previous section. The transmission, reflection, and total absorption coefficients plotted as a function of the parallel wave number are shown in Fig. 9. The shape of the curves for $k_{\|}<5.5$ m^{-1} is indicative of a Budden (resonance–cutoff) configuration, whereas for $k_{\|}>5.5$ m^{-1}, the oscillations in the reflection and total absorption indicate that the high-field, fast wave cutoff is now present in the plasma, thus, producing the triplet (cutoff–resonance–cutoff) configuration. Notice that the reflection coefficient drops to 10% for $k_{\|}=8.5$ m^{-1}. However, although this low reflection is associated with 90% absorption, the curve does not indicate how this absorbed energy is divided between mode conversion and direct dissipation by the ions and electrons.

This question can be answered by referring to Eq. (30) for the total absorption. The energy mode converted can be obtained from the fast wave equation by integrating Im $Q(x)|E_y|^2$ only over the hybrid resonance. This provides a reliable guide to the mode converted fraction in this special case of comparable ion concentrations, where the ion cyclotron resonance regions are well separated from the two-ion hybrid resonance. This procedure is illustrated in Fig. 10, in which the total absorption curve is compared with the con-

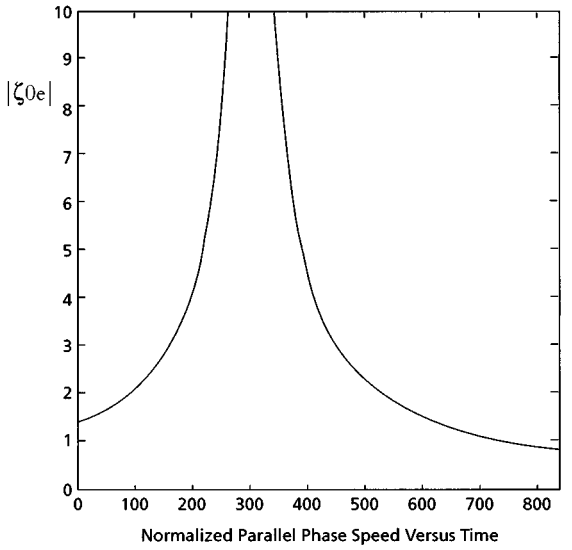

FIG. 8. The change in the normalized parallel phase speed $\zeta_{oe}=\omega/k_{\|}v_{Te}$ along the ion hybrid ray trajectory. The parameters are the same as Fig. 5.

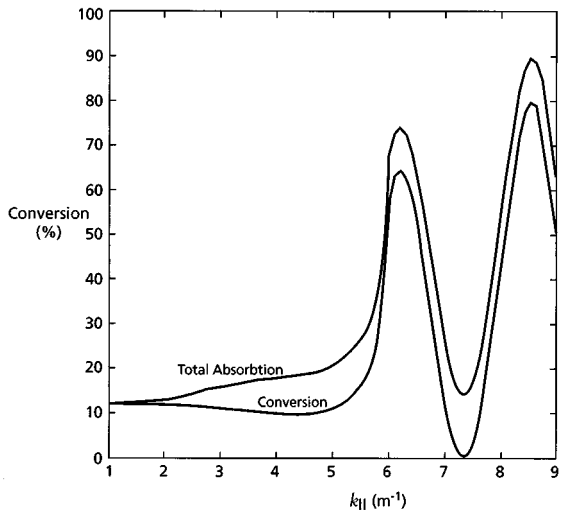

FIG. 10. Comparison of total absorption with the mode converted power plotted as a function of the parallel wave number. The parameters are the same as in Fig. 9.

Downloaded 31 Oct 2012 to 194.81.223.66. Redistribution subject to AIP license or copyright; see http://pop.aip.org/about/rights_and_permissions

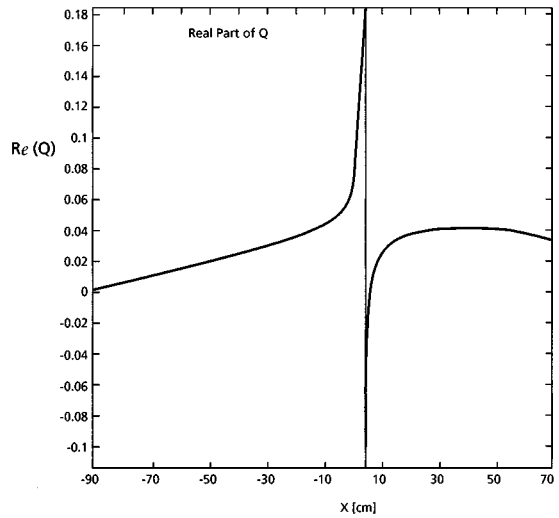

FIG. 11. The real part of the fast wave potential [Eq. (28)] plotted as a function of the spatial coordinate. The parameters are the same as Fig. 9 with $k_{\|}=5\ \mathrm{m}^{-1}$.

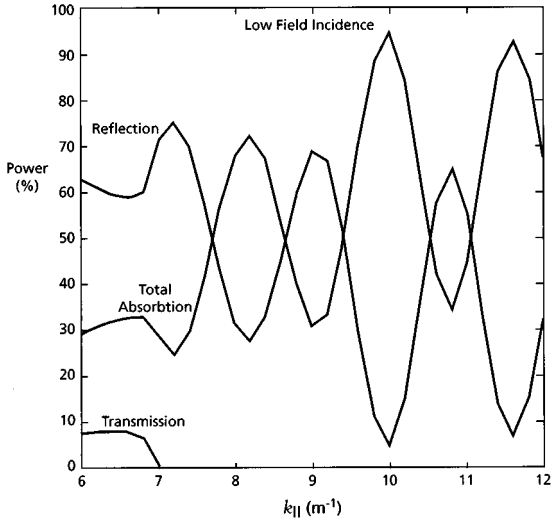

FIG. 13. Transmission, reflection, and total absorption fractions plotted as a function of the parallel wave number for TFTR parameters: $n_e=5\times10^{19}\ \mathrm{m}^{-3}$, $B_0=4.8$ T, $R=2.62$ m, $T_e=10$ keV for a deuterium (51%)–tritium (49%) plasma with $T_{\mathrm{D}}=T_{\mathrm{T}}=20$ keV.

version integral, again plotted as a function of the parallel wave number. It can be seen that the fraction mode converted can be as high as 80% under optimum conditions, with 10% of the power dissipated outside the resonance region. The real and imaginary parts of the fast wave potential are shown in Figs. 11 and 12. The real part shows the characteristic shape with the resonance on the high-field side and the cutoff on the low-field side. The imaginary part of the potential shows the two cyclotron resonances broadened by the Doppler spread of thermal ions and the central, very sharp, hybrid resonance. The imaginary part, which occurs as a weak background damping over the whole plasma, is, of course, the direct electron fast wave damping.

A similar set of results is shown in Figs. 13–16 for TFTR parameters. Here, the electron density was taken as $5\times10^{19}\ \mathrm{m}^{-3}$ and a deuterium–tritium plasma with 51% deuterium and 49% tritium was assumed. The magnetic field was taken as 4.8 T, the major radius 2.62 m, and the electron and ion temperatures 10 and 20 keV, respectively. The transmission, reflection, and absorption coefficients shown in Fig. 13 indicate the triplet behavior for almost the whole range of the parallel wave number. The mode converted power can be as high as 75%, as shown in Fig. 14. In this higher temperature case, the damping outside the two-ion hybrid resonance region is stronger, but still only 15%. The curves for the real and imaginary parts of the potential, shown in Figs. 15 and 16, are similar to the previous example, although the ion cyclotron resonances are broader due to the higher ion temperatures.

In the final example, given in Figs. 17–20, the same TFTR parameters have been used, except the electron density is increased to $2\times10^{20}\ \mathrm{m}^{-3}$ and the electron temperature

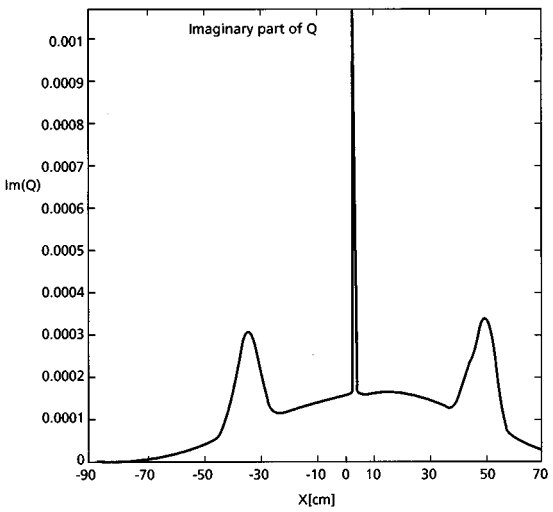

FIG. 12. The imaginary part of the fast wave potential plotted as a function of the spatial coordinate. The parameters are the same as Fig. 9 with $k_{\|}=5\ \mathrm{m}^{-1}$.

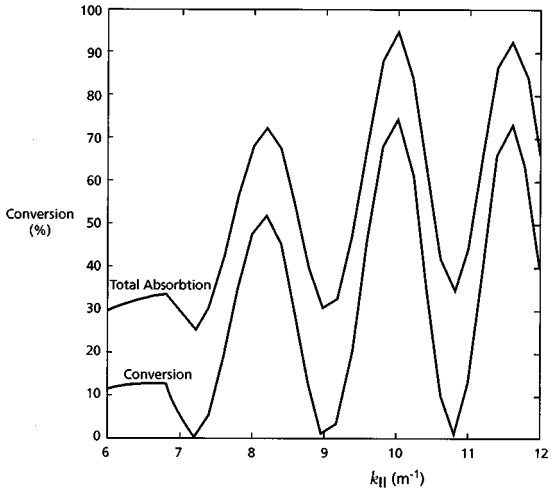

FIG. 14. Comparison of total absorption with the mode converted power plotted as a function of the parallel wave number. The parameters are the same as Fig. 13.

Downloaded 31 Oct 2012 to 194.81.223.66. Redistribution subject to AIP license or copyright; see http://pop.aip.org/about/rights_and_permissions

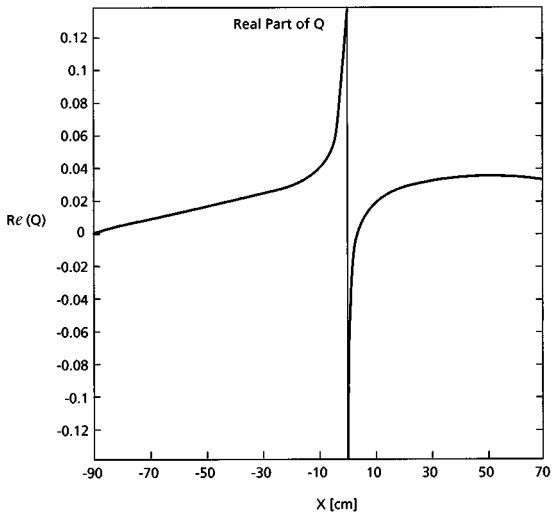

FIG. 15. The real part of the fast wave potential plotted as a function of the spatial coordinate. The parameters are the same as Fig. 13 with $k_{\|} = 6.6\ \mathrm{m}^{-1}$.

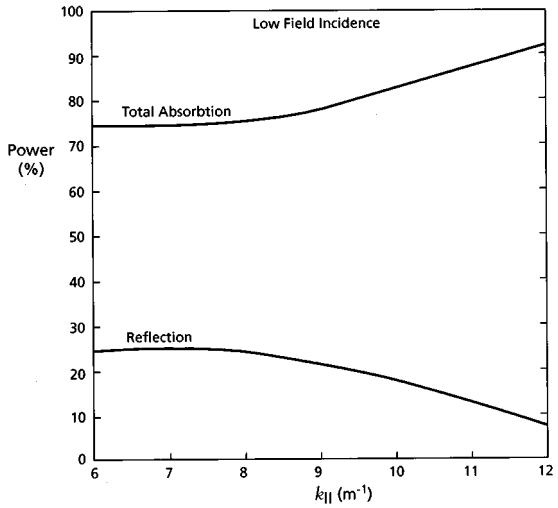

FIG. 17. Transmission, reflection, and total absorption fractions plotted as a function of the parallel wave number for TFTR projected parameters: $n_e = 2\times10^{20}\ \mathrm{m}^{-3}$, $B_0 = 4.8$ T, $R = 2.62$ m, $T_e = 30$ keV for a deuterium (51%)–tritium (49%) plasma with $T_\mathrm{D} = T_\mathrm{T} = 20$ keV.

taken as 30 keV, which represents an increase in the electron beta of a factor 12. In this case, Fig. 17 shows a behavior of the transmission, reflection, and absorption coefficients, which is characteristic of the Budden configuration. The transmission is zero for the whole range of the parallel wave number and the total absorption always above 75%. Now, however, the mode converted energy, shown in Fig. 18, is extremely small so that the absorption occurs on the low-field side of the resonance. The real part of the potential, Fig. 19, is similar to the other cases, but the imaginary part of the potential, Fig. 20, shows a greatly enhanced electron damping, with the hybrid resonance barely visible.

VIII. SUMMARY AND CONCLUSIONS

We have described the properties of ion-Bernstein waves in a plasma containing two-ion species, highlighting the special role of the ion hybrid wave. In particular, the ion hybrid wave is much less susceptible to ion cyclotron damping than ion-Bernstein waves in the region where these waves couple to the fast wave. A general analytic expression for the transmission coefficient of the fast wave across the two-ion hybrid resonance has been given. This is valid for any concentration ratio of the two ion species and is relevant to both the Budden and triplet configurations. A formula for the local electron Landau damping rate of the ion hybrid wave has

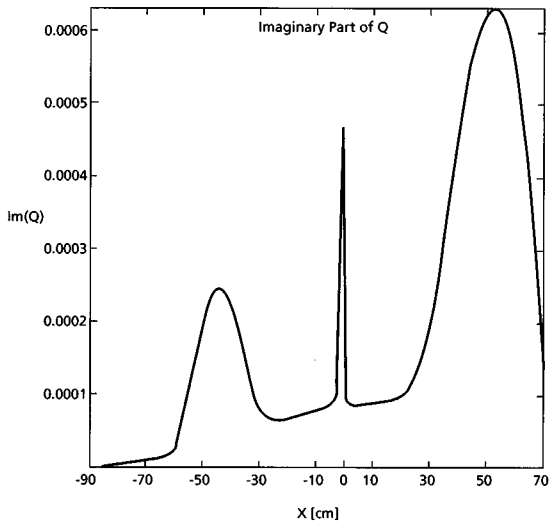

FIG. 16. The imaginary part of the fast wave potential plotted as a function of the spatial coordinate. The parameters are the same as Fig. 13 with $k_{\|} = 6.6\ \mathrm{m}^{-1}$.

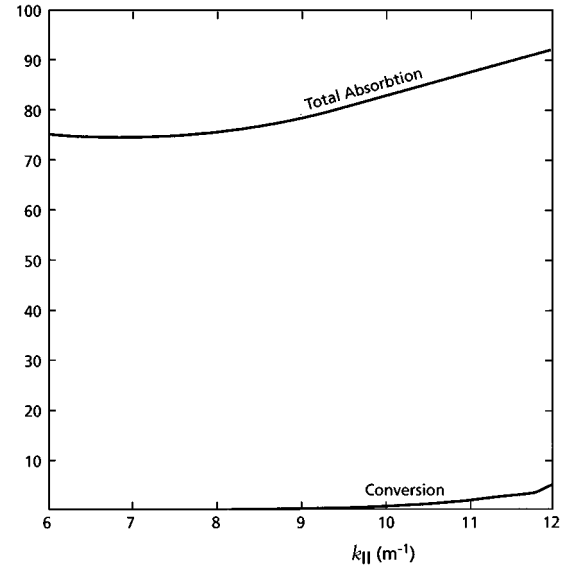

FIG. 18. Comparison of total absorption with the mode converted power plotted as a function of the parallel wave number. The parameters are the same as Fig. 17.

Downloaded 31 Oct 2012 to 194.81.223.66. Redistribution subject to AIP license or copyright; see http://pop.aip.org/about/rights_and_permissions

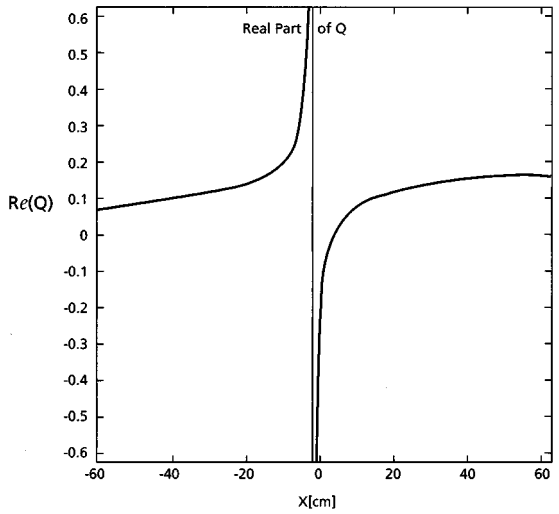

FIG. 19. The real part of the fast wave potential plotted as a function of the spatial coordinate. The parameters are the same as Fig. 17 with $k_{\|} = 6.6\ \mathrm{m}^{-1}$.

been derived and found to be in good agreement with the numerical result obtained from the exact linear dispersion relation.

For plasmas with two ion species present in comparable concentrations, ion cyclotron damping of the fast wave can be reduced by polarization effects. Integration of the second-order fast wave equation, containing all the damping mechanisms, provides an efficient numerical scheme to quantify the competition between mode conversion and damping of the fast wave outside the region of the two-ion hybrid resonance. For future scenarios on large tokamaks, such as JET, TFTR, and ITER, we have noted optimum conditions for mode conversion and have also quantified the requirement on the electron beta such that the fast Alfvén wave is absorbed directly by the electrons and no power is mode converted. Hence, the fast wave can be used to produce strong single pass electron heating regardless of the electron beta. For low electron beta, strong electron heating can occur via mode conversion, a result which has been convincingly demonstrated on TFTR.[4] For high beta, strong single pass electron heating by direct damping of the fast Alfvén wave can occur.

The understanding obtained of strong electron heating through mode conversion to the ion hybrid wave should enable a much more systematic investigation of fast wave–lower hybrid synergy[21] to be carried out. The study of non-inductive current drive by the mode converted ion hybrid waves has already begun on TFTR. The accessibility properties of the fast wave and the control of the absorption position through the two-ion hybrid resonance, make this a promising avenue for future investigations. Further theoretical analysis is clearly required.

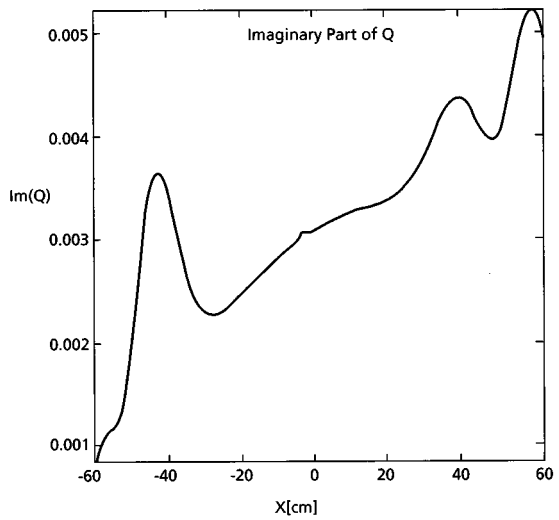

FIG. 20. The imaginary part of the fast wave potential plotted as a function of the spatial coordinate. The parameters are the same as Fig. 17 with $k_{\|} = 6.6\ \mathrm{m}^{-1}$.

ACKNOWLEDGMENTS

One of the authors (C. N. Lashmore-Davies) would like to thank Dr. V. P. Bhatnagar for useful discussions. The authors would also like to thank Mr. E. Oliver who computed Figs. 1 and 2.

This work was partly supported by the U.K. Department of Trade and Industry and Euratom, by the Centre Canadien de Fusion Magnétique (CCFM) and by the U.S. Department of Energy Contract No. DE-FG02-91-ER-54109. CCFM is jointly managed and funded by Atomic Energy of Canada Limited, Hydro-Québec, and the Institut National de Recherche Scientifique.

APPENDIX: FINITE LARMOR RADIUS DISPERSION RELATION IN THE TWO-ION HYBRID RESONANCE REGION

In this appendix we derive the finite Larmor radius dispersion relation for a plasma containing two-ion species in comparable proportions. We start from Eq. (31), but neglect the electron damping terms on the right-hand side, and substitute Eqs. (3)–(5) for the dielectric tensor elements, in which the plasma dispersion functions for the ions are expanded asymptotically, assuming $(\omega - n\Omega_j)/k_{\|} v_{Tj} \gg 1$ for both ion species. The dispersion relation is, therefore, relevant to the region of the two-ion hybrid resonance when this resonance is well separated from the cyclotron resonances of the two-ion species. In other words, the dispersion relation is most accurate for the case when the two-ion species are present in approximately equal proportions. Retaining terms to first order in $k_{\perp}^2 \rho_j^2$ for both ion species, we multiply through Eq. (31) by

$$\left(\frac{\Omega_1^2}{\omega_{p1}^2}\right)^2 (\Omega_1^2 - \omega^2)(\omega^2 - \Omega_2^2)\, \frac{\omega^2}{\Omega_1^2} \left(1 + \frac{\omega_{p2}^2}{\omega_{p1}^2}\right)^{-1} \left(1 + \frac{\rho_2}{\rho_1}\right)^{-1},$$

and after some algebraic manipulation we obtain the dispersion relation

Downloaded 31 Oct 2012 to 194.81.223.66. Redistribution subject to AIP license or copyright; see http://pop.aip.org/about/rights_and_permissions

$$
\begin{aligned}
&(\omega^2-c_A^2k_\perp^2)\Bigg\{\omega^2-\Omega_{ii}^2+\frac{N_\parallel^2(\omega^2/\Omega_1^2-1)(\omega^2-\Omega_2^2)(1+\rho_2/\rho_1)}{(1+\omega_{p2}^2/\omega_{p1}^2)}-\frac{1}{2(1+\omega_{p2}^2/\omega_{p1}^2)}\Bigg[\omega^2-\Omega_2^2+\frac{\omega_{p2}^2}{\omega_{p1}^2}(\omega^2-\Omega_1^2)\frac{v_{T2}^2}{v_{T1}^2}\frac{\Omega_1^2}{\Omega_2^2}\\
&\quad-\frac{(\omega^2-\Omega_1^2)(\omega^2-\Omega_2^2)}{(\omega^2-4\Omega_1^2)}-\frac{\omega_{p2}^2}{\omega_{p1}^2}\frac{(\omega^2-\Omega_1^2)(\omega^2-\Omega_2^2)}{(\omega^2-4\Omega_2^2)}\frac{v_{T2}^2}{v_{T1}^2}\frac{\Omega_1^2}{\Omega_2^2}\Bigg]\frac{k_\perp^2v_{T1}^2}{\Omega_1^2}\Bigg\}\\
&=\frac{\omega^2}{(1+\omega_{p2}^2/\omega_{p1}^2)}\Bigg\{\frac{\omega_{p2}^2}{\omega_{p1}^2}\frac{(\Omega_1-\Omega_2)^2}{(1+\rho_2/\rho_1)}\frac{\omega^2}{\Omega_2^2}+2N_\parallel^2(\omega^2-\Omega_2^2)+2N_\parallel^2\frac{\omega_{p2}^2}{\omega_{p1}^2}(\omega^2-\Omega_1^2)+\frac{N_\parallel^4}{\Omega_1^2}(\omega^2-\Omega_1^2)(\omega^2-\Omega_2^2)\Bigg(1+\frac{\rho_2}{\rho_1}\Bigg)\\
&\quad+N_\parallel^2\Bigg(\frac{\omega^2}{\Omega_1^2}-1\Bigg)(\omega^2-\Omega_2^2)\Bigg(1+\frac{\rho_2}{\rho_1}\Bigg)\\
&\quad-\Bigg[\frac{(\omega^2-\Omega_2^2)}{(1+\rho_2/\rho_1)}+\frac{\omega_{p2}^2}{\omega_{p1}^2}\frac{(\omega^2-\Omega_1^2)}{(1+\rho_2/\rho_1)}+\frac{N_\parallel^2(\omega^2-\Omega_1^2)(\omega^2-\Omega_2^2)}{\Omega_1^2}\Bigg]\Bigg[\frac{2\Omega_1^2}{(\omega^2-\Omega_1^2)}+\frac{2\omega_{p2}^2}{\omega_{p1}^2}\frac{\Omega_1^2}{(\omega^2-\Omega_1^2)}\frac{v_{T2}^2}{v_{T1}^2}\frac{\Omega_1^2}{\Omega_2^2}-\frac{\Omega_1^2}{(\omega^2-4\Omega_1^2)}\\
&\quad-\frac{\omega_{p2}^2}{\omega_{p1}^2}\frac{\Omega_1^2}{(\omega^2-4\Omega_2^2)}\frac{v_{T2}^2}{v_{T1}^2}\frac{\Omega_1^2}{\Omega_2^2}-\frac{\Omega_1^2}{\omega^2}-\frac{\omega_{p2}^2}{\omega_{p1}^2}\frac{\Omega_1^2}{\omega^2}\frac{v_{T2}^2}{v_{T1}^2}\frac{\Omega_1^2}{\Omega_2^2}\Bigg]\frac{k_\perp^2v_{T1}^2}{\Omega_1^2}-2\Bigg[\frac{(\omega^2-\Omega_2^2)\omega}{(1+\rho_2/\rho_1)\Omega_1}+\frac{\omega_{p2}^2}{\omega_{p1}^2}\frac{(\omega^2-\Omega_1^2)\omega}{(1+\rho_2/\rho_1)\Omega_2}\Bigg]\\
&\quad\times\Bigg[-\frac{\Omega_1^2}{(\omega^2-\Omega_1^2)}\frac{\Omega_1}{\omega}-\frac{\omega_{p2}^2}{\omega_{p1}^2}\frac{\Omega_1^2}{(\omega^2-\Omega_2^2)}\frac{\Omega_2}{\omega}\frac{v_{T2}^2}{v_{T1}^2}\frac{\Omega_1^2}{\Omega_2^2}+\frac{\Omega_1^2}{(\omega^2-4\Omega_1^2)}\frac{\Omega_1}{\omega}+\frac{\omega_{p2}^2}{\omega_{p1}^2}\frac{\Omega_1^2}{(\omega^2-4\Omega_2^2)}\frac{\Omega_2}{\omega}\frac{v_{T2}^2}{v_{T1}^2}\frac{\Omega_1^2}{\Omega_2^2}\Bigg]\frac{k_\perp^2v_{T1}^2}{\Omega_1^2}\\
&\quad+\frac{1}{2}\Bigg[\omega^2-\Omega_2^2+\frac{\omega_{p2}^2}{\omega_{p1}^2}(\omega^2-\Omega_1^2)\frac{v_{T2}^2}{v_{T1}^2}\frac{\Omega_1^2}{\Omega_2^2}-\frac{(\omega^2-\Omega_1^2)(\omega^2-\Omega_2^2)}{(\omega^2-4\Omega_1^2)}-\frac{\omega_{p2}^2}{\omega_{p1}^2}\frac{(\omega^2-\Omega_1^2)(\omega^2-\Omega_2^2)}{(\omega^2-4\Omega_2^2)}\frac{v_{T2}^2}{v_{T1}^2}\frac{\Omega_1^2}{\Omega_2^2}\Bigg]\frac{k_\perp^2v_{T1}^2}{\Omega_1^2}\Bigg\}. \qquad \text{(A1)}
\end{aligned}
$$

We reiterate that $c_A^2=B_0^2/\mu_0(\rho_1+\rho_2)$ and $N_\parallel^2=c_A^2k_\parallel^2/\omega^2$. The dispersion relation given in Eq. (A1) includes both the ion hybrid wave and the fast wave. The specific dispersion relations given in Eqs. (32) and (36) were obtained from Eq. (A1) with the addition of the second term on the right-hand side of Eq. (31), which describes the damping of the ion hybrid wave.

[1] *Technical Basis for the ITER Interim Design Report, Cost Review and Safety Analysis* (International Atomic Energy Agency, Vienna, 1996).

[2] A. K. Ram, A. Bers, and V. Fuchs, *Proceedings of the 20th EPS Conference on Controlled Fusion and Plasma Physics*, Lisboa, Portugal, 1993, edited by J. A. Costa Cabral, M. E. Manso, F. M. Serra, and F. C. Schüller (European Physical Society, Petit-Lancy, 1993), Vol. 17C, Part III, pp. 897–900.

[3] J. Jacquinot, B. D. McVey, and J. E. Scharer, Phys. Rev. Lett. **29**, 88 (1977).

[4] R. Majeski, C. K. Phillips, and J. R. Wilson, Phys. Rev. Lett. **73**, 2204 (1994); R. Majeski, J. C. Hosea, C. K. Phillips, J. H. Rogers, G. Schilling, J. E. Stevens, and J. R. Wilson, *10th Topical Conference on Radio Frequency Power in Plasmas 1993*, Boston, AIP Conf. Proc. No. 289, edited by M. Porkolab and J. Hosea (American Institute of Physics, New York, 1993), p. 401.

[5] K. G. Budden, in *The Propagation of Radio Waves* (Cambridge University Press, Cambridge, 1985), p. 596.

[6] V. Fuchs, A. K. Ram, S. D. Schultz, A. Bers, and C. N. Lashmore-Davies, Phys. Plasmas **2**, 1637 (1995).

[7] A. K. Ram, A. Bers, S. D. Schultz, and V. Fuchs, Phys. Plasmas **3**, 1976 (1996).

[8] M. Brambilla and M. Ottaviani, Plasma Phys. Controlled Fusion **27**, 1 (1986).

[9] D. G. Swanson, Phys. Fluids **28**, 2645 (1985).

[10] D. J. Grove and D. M. Meade, Nucl. Fusion **25**, 1167 (1985).

[11] The Joint European Torus Team, Nucl. Fusion **32**, 187 (1992).

[12] T. H. Stix, in *Waves in Plasmas* (American Institute of Physics, New York, 1992), p. 257.

[13] M. Ono, Phys. Rev. Lett. **42**, 1267 (1979).

[14] A. I. Akhiezer, I. A. Akhiezer, R. V. Polovin, A. G. Sitenko, and K. N. Stepanov, in *Plasma Electrodynamics* (Pergamon, Oxford, 1975), Vol. I, p. 284.

[15] C. K. Chow, A. K. Ram, and A. Bers, Phys. Fluids B **1**, 2018 (1989).

[16] Y. C. Ngan and D. G. Swanson, Phys. Fluids **20**, 1920 (1977).

[17] B. Saoutic, A. Bécoulet, T. Hutter, D. Fraboulet, A. K. Ram, and A. Bers, Phys. Rev. Lett. **76**, 1647 (1996).

[18] M. Porkolab, in *Radio Frequency Power in Plasmas*, Charleston, SC 1991, AIP Conf. Proc. No. 288, edited by D. B. Batchelor (American Institute of Physics, New York, 1992), p. 197.

[19] A. K. Ram and A. Bers, Phys. Fluids B **3**, 1059 (1991).

[20] M. Ono, Phys. Fluids B **5**, 241 (1993).

[21] The Joint European Torus Team (presented by C. Gormezano), in *Plasma Physics and Controlled Nuclear Fusion Research*, 1992, Würzburg (International Atomic Energy Agency, Vienna, 1993), Vol. I, p. 587.

Downloaded 31 Oct 2012 to 194.81.223.66. Redistribution subject to AIP license or copyright; see http://pop.aip.org/about/rights_and_permissions